

Digital image correlation techniques applied to post-process discrete modeling

A. Delaplace & F. Hild

LMT-Cachan, ENS de Cachan / CNRS UMR 8535 / Université Paris 6

ABSTRACT: The present work focuses on post-processing discrete modeling. Discrete models are used to describe failure of brittle and heterogeneous material. By noting that data obtained with these models are very close to those obtained with digital image correlation techniques (displacement fields), similar algorithms are applied to compute usual data such as strain fields. Different examples illustrate performances of the approach, in particular regarding the computation of stress intensity factors.

1 INTRODUCTION

Discrete element models are widely used for computing failure of cementitious and concrete structures, thanks to modern computer performance. However, engineering applications with discrete descriptions are still uncommon in comparison with finite element techniques. One of the reasons for this is that homogenized quantities (e.g. stress, strain, damage variables), usually “handled” by engineers are not naturally obtained with discrete descriptions: such an approach is based on a description of the material microstructure that accounts for heterogeneities. Discrete models deal only with local quantities, and require averages to be performed for macroscale analyses. Different solutions to the averaging problem have been proposed, mainly based on spatial averages of the local quantities.

We propose here a more general approach, based on image correlation techniques. During the last years, these techniques have become very attractive for analyzing experimental tests (Sutton et al. 2000). Local and global quantities are obtained all over the sample by measuring kinematic changes between two states. Depending on the material behavior, one can measure displacement fields, or identify strain fields, or even stress intensity factors, for example. The analysis is performed on a heterogeneous field from the evaluation of local quantities, a feature also present in discrete models. Following this idea, the same type of analysis for both experimental tests and discrete modeling computations is performed to obtain mechanical fields. We illustrate this post-processing technique on several examples of building materials and concrete structures.

In the first part, we present the discrete model used in this study, with a particular focus on the standard

post-processing tools. Extensions to discrete modeling are proposed, and applications on strain field will be shown to illustrate the performance of the approach. A last example of crack propagation in a beam is introduced, with an estimation of stress intensity factors.

2 DISCRETE MODEL

2.1 Model basis

In the framework of discrete modeling, the material is not described as a continuous medium but as an assembly of particles. This assembly may break under loading, allowing a natural description of discontinuities. Hence, these discrete models are relevant to represent failure of brittle heterogeneous material, caused by nucleation, propagation and coalescence of cracks. In this study, the material is described by an assembly of rigid cells, obtained from a Voronoi tessellation computed on a set of randomly distributed points (see for instance (Tillemans and Herrmann 1995)). Centers of neighboring particles are linked together by Euler-Bernoulli beams (figure 1) in order to represent the elastic behavior of an isotropic medium, characterized by two elastic parameters. Inelastic response of material is obtained by introducing a nonlinear behavior for the beams. We choose here an elastic-brittle law to describe the response of a quasi-brittle material such as concrete. The failure threshold P_{ij} for beam ij is computed from

$$P_{ij} \left(\frac{\varepsilon_{ij}}{\varepsilon_{ij}^{cr}}, \frac{|\psi_i - \psi_j|}{\psi_{ij}^{cr}} \right) \geq 1 \quad (1)$$

where ε_{ij}^{cr} and ψ_{ij}^{cr} are considered to be random variables with Gaussian distribution, ε_{ij}^{cr} corresponds to the failure of the beam in tensile mode, and ψ_{ij}^{cr} cor-

responds to the failure of the beam in a bending mode (Woestyn et al. 2006). Microstructure heterogeneities are then introduced through the mesh variability and through the probability density function of ε_{ij}^{cr} and ψ_{ij}^{cr} . At this point, the model is nothing

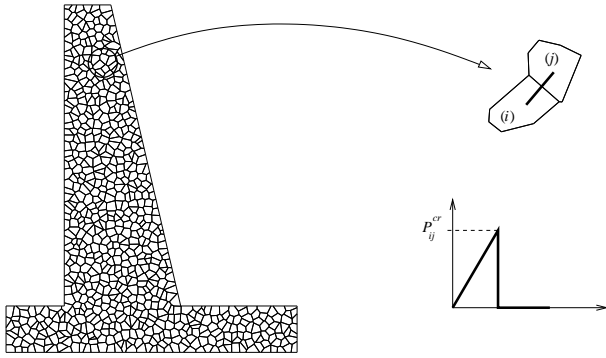


Figure 1. Example of Voronoi mesh.

but a lattice model (Schlangen and Garboczi 1997; Van Mier et al. 2002). Particle shapes are taken into account in two cases:

- When two disconnected particles overlap, a contact force is generated. This force depends on the area of the overlap domain, and therefore on particle shapes.
- For dynamic loadings, Voronoi shapes are needed to estimate the weight distribution of particles to compute the mass matrix.

In the following, quasi-static loadings are considered with the following elastic prediction algorithm (Deplaplace and Rey 2005):

Step k

1. apply elastic loading \mathbf{f}^{el}
2. compute \mathbf{u}^{el} using an iterative method
3. compute α_{\min} with

$$\alpha_{\min} = \min_{\substack{i,j \in (1,\dots,n) \\ i \neq j}} \left(\frac{1}{P_{ij}} \right)$$

4. save couple $(\alpha_{\min} \mathbf{u}^{el}, \alpha_{\min} \mathbf{f}^{el})$
5. change stiffness matrix with

$$\mathbf{K}^{k+1} = \mathbf{K}^k - \mathbf{L}_{ij}^T \mathbf{K}_{ij} \mathbf{L}_{ij}$$

where \mathbf{L}_{ij} is the connectivity matrix of element ij .

End step k

This algorithm allows one to follow snap back responses and solution uniqueness is guaranteed.

2.2 Basic post-processing

Different elementary outputs are produced when running numerical simulations:

- a force-displacement curve,
- the crack pattern or damaged zones for a brittle material,
- the displacement field.

These outputs are obtained directly, without any interpretation or transformation. Figures 2 and 3 show such outputs for a discrete model. A 3-point bend simulation is performed on a 0.8×0.1 m beam. The mesh is made of 160×20 particles. The Gaussian distributions of the model random parameters are characterized by the average and the standard-deviation of each values:

$$\bar{\varepsilon}_{cr} = 1.5 \times 10^{-4} \quad \sigma_{\varepsilon_{cr}} = 0.05$$

$$\bar{\theta}_{cr} = 5.6 \times 10^{-3} \quad \sigma_{\theta_{cr}} = 0.05,$$

As expected, a vertical macrocrack propagates from the bottom face of an initially uncracked beam.

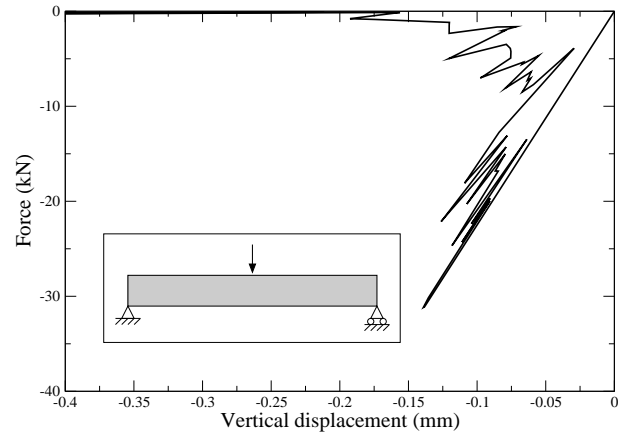


Figure 2. Force-displacement response.

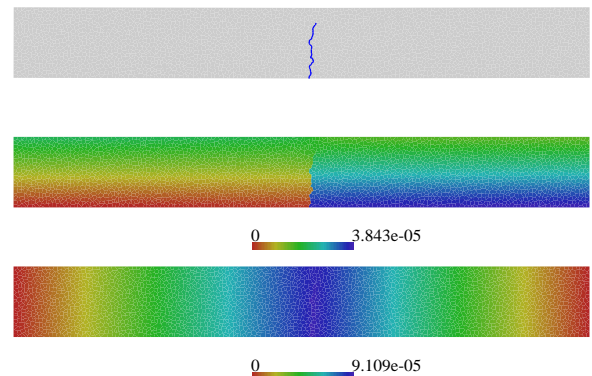


Figure 3. Crack pattern, horizontal and vertical displacements of the 3-point bend configuration.

However, one may need more refined data from the simulation. For instance, strain and stress fields

are usually needed by engineers. More specifically, stress intensity factors are a basic quantity for fracture mechanics analyses, as is the damage field for damage mechanics. This information is not be obtained directly from a simulation. Some “transformations” are to be performed from the computed displacement field. These transformations are the key for a good interpretation of simulation results, especially for heterogeneous materials. A first possibility consists in computing the different quantities close to the particle scale, *e.g* the strain field is computed by averaging the displacements of the beams connected to each particle. This approach has the virtue of being simple, but is not necessarily relevant in terms of scale. One may imagine obtaining information at a coarser scale than that of the particles. This is achieved by considering mechanical solutions of the studied problem. Analytical solutions of basic problems are known and can be used to enrich the computation of a strain field from a discrete displacement field. This kind of consideration has been developed successfully during the last years for experimental measurements, for instance by using digital image correlation techniques (Roux and Hild 2006).

By noting that data obtained from a discrete element model computation and from a experimental digital image correlation result are very similar (a discrete displacement field), we propose to apply DIC algorithms to post-process discrete modeling. We propose in the next part to illustrate enhanced postprocess output obtained with such an analysis.

3 STRAIN ANALYSIS

Computing strain fields from displacement field is a problem that has been studied for several years (Allais et al. 1994; Geers et al. 1996; Kruyt and Rothenburg 1996). For heterogeneous materials, computing local strains from displacement on the boundary of a considered domain is common to experimental and numerical applications. The average strain tensor ε is computed over a domain ω with

$$\varepsilon = \frac{1}{V_\omega} \int_{\partial\omega} \frac{1}{2} (\mathbf{u} \otimes \mathbf{n} + \mathbf{n} \otimes \mathbf{u}) ds$$

where \mathbf{u} is the displacement of a material point in the studied configuration, \mathbf{n} the normal to the domain boundary $\partial\omega$ and V_ω is the area of the domain. Strain values are expected to be independent of domain ω if its size is large with respect to the material microstructure scale (or particle size for discrete model). This condition is not fulfilled for this study. Therefore, strain fields depend in part on the size and the shape of the domain ω , and different choices are possible (figure 4). Following (D’Adetta et al. 2004), we choose a circular domain with a diameter of about five times the particle size.

Strain fields are computed on a square sample loaded vertically in tension (64×64 particles). Model parameters are identical to that of the first example.

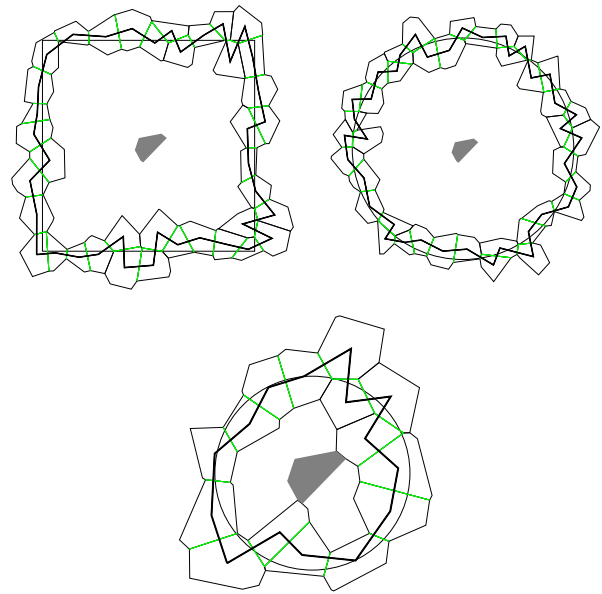


Figure 4. Different sizes and shapes of domain boundary $\partial\omega$ (bold line) for a Voronoi particle (grey filled). The following computations use the last domain.

The failure mode corresponds to a macrocrack that propagates through the sample, perpendicular to the loading direction. Note that the vertical position of the macrocrack is *a priori* unknown. Strain fields ε_{11} (horizontal), ε_{22} (vertical) and ε_{12} are plotted in figure 5 (note the different scales), where a fixed range is used. Strong discontinuity due to the macrocrack is clearly visible, as the regularization due to the average computation on the domain boundary. Changes of strain fields ε_{22} with the crack propagation is shown in figure 6, with an adaptive range for the gray scale.

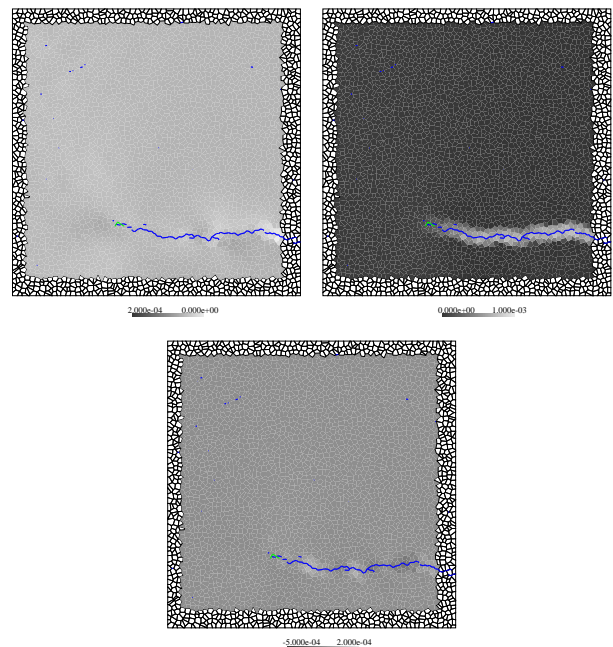


Figure 5. Strain ε_{11} , ε_{22} and ε_{12} fields for a simple tension test.

The spatial resolution of the strain fields is limited with this approach to the particle size (just one value

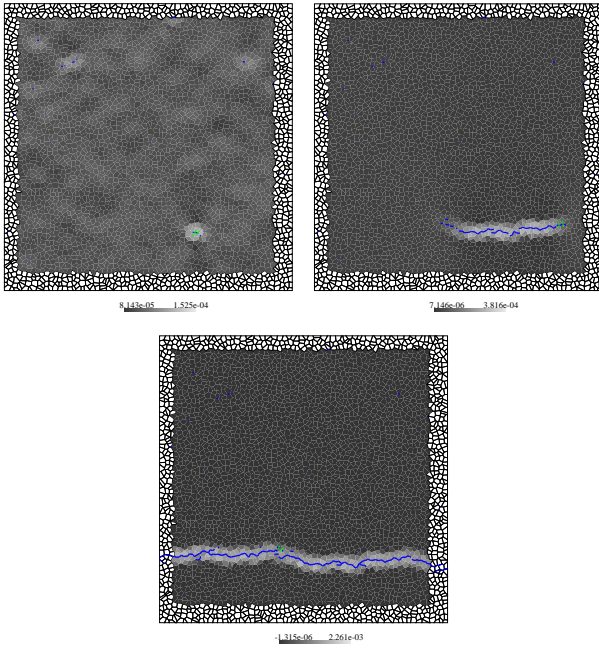


Figure 6. Change of strain field ε_{22} with crack propagation (adaptive range scale).

is computed for each particle). This limitation vanishes if one considers integrating this field over the particle area. For elastic problems, a simple linear integration is the best approximation of the strain field.

4 STRESS INTENSITY FACTOR EVALUATION

Extracting some mechanically meaningful information using the detailed map of displacement is performed by identifying the amplitudes of relevant reference displacement fields. In the present case, one can easily list some meaningful contributions. First, rigid body motions have to be accounted for and constitute the first three fields, two in-plane translations, \mathbf{v}_1 and \mathbf{v}_2 , and one rotation about an axis normal to the observation plane, \mathbf{v}_3 . One single uniform strain field, \mathbf{v}_4 , is allowed for in order to leave the crack face stress-free, the so-called ‘‘T-stress’’ (uniaxial tension along the crack direction). The presence of a crack generates two independent ‘‘singular’’ displacement fields corresponding to modes I, \mathbf{v}_5 , and II, \mathbf{v}_6 , with two scalar amplitudes that will give access to the stress intensity factors. Lastly, in order to enrich the basis, one may also consider the next order sub-singular mode I and II fields, respectively denoted by \mathbf{v}_7 and \mathbf{v}_8 . It is convenient to express these vectors as complex valued fields in the local crack frame (crack tip at the origin, and crack extension along the negative real axis). A current point M is represented by a complex number $z = x + iy$ or polar coordinates $z = re^{i\theta}$, and similarly the displacement is represented by $\mathbf{u} = u_x + iu_y$. The expression of the eight

basis functions is

$$\begin{aligned}
 \mathbf{v}_1(z) &= 1 \\
 \mathbf{v}_2(z) &= i \\
 \mathbf{v}_3(z) &= iz \\
 \mathbf{v}_4(z) &= (\kappa - 1)z + 2\bar{z} \\
 \mathbf{v}_5(z) &= \sqrt{r}[2\kappa e^{i\theta/2} - e^{3i\theta/2} - e^{-i\theta/2}] \\
 \mathbf{v}_6(z) &= i\sqrt{r}[2\kappa e^{i\theta/2} + e^{3i\theta/2} - 3e^{-i\theta/2}] \\
 \mathbf{v}_7(z) &= \sqrt{r^3}[2\kappa e^{3i\theta/2} - 3e^{i\theta/2} + e^{-3i\theta/2}] \\
 \mathbf{v}_8(z) &= i\sqrt{r^3}[2\kappa e^{3i\theta/2} + 3e^{i\theta/2} - 5e^{-3i\theta/2}]
 \end{aligned} \tag{2}$$

where

$$\kappa = \frac{(3 - \nu)}{(1 + \nu)} \tag{3}$$

in plane stress condition, as expected along the free (examination) surface, with ν being the Poisson’s ratio. Let us note however that the amplitudes of these functions are real numbers.

The strategy is thus to decompose the estimated displacement field (from discrete calculations, see Fig. 3) onto the basis of \mathbf{v}_k test functions. For this goal, the following objective function is minimized

$$\mathcal{T}(a) = \sum_{i=1}^{N_{co}} \left\| \mathbf{u}_i - \sum_k a_k \mathbf{v}_k \right\|^2 \tag{4}$$

where N_{co} is the number of computed displacement points.

One advantage of this formulation is that the value reached by the objective function constitutes a global quality parameter. Since the identification procedure assumes that the crack geometry is known, a minimization of this global residual over the *a priori* guessed crack tip position also provides a natural way of optimizing the crack geometry. It can be noted that other techniques can be followed to extract the stress intensity factor by using interaction integrals (Hellen 1975; Destuynder and Djaoua 1981; Réthoré et al. 2005).

This identification is carried out on the 3-point bending test presented in Section 2.2. The results reported below are obtained from estimates of the displacement field over a region of interest that amounts to a disk of external radius of 0.03 m centered on a gross determination of the crack tip position. In figure 7, the map of estimated mode I and mode II stress intensity factors is plotted as functions of the guessed crack tip location (for output convenience, the beam axis is vertical). To select the most appropriate location, the map of global residual is shown in the same figure. The crack tip is accurately located in both directions. From the absolute minimum, one locates quite precisely the crack tip position that provides the best fit quality. The position of the crack tip estimated by the post-processing approach is $x = 0.385$ m and $y = 0.049$ m. These values are in very good agreement with the ‘‘real’’ crack tip position $x = 0.383$ m and $y = 0.048$ m, which correspond to the last broken beam location.

computation of stress intensity factors is performed on a three-point bending test problem.

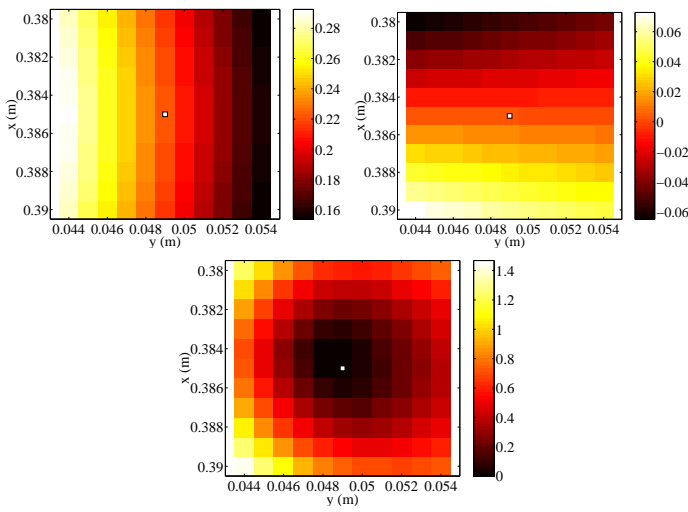


Figure 7. K_I in $\text{MPa}\sqrt{\text{m}}$ (left), K_{II} in $\text{MPa}\sqrt{\text{m}}$ (center) and global residual $(\mathcal{T} - \mathcal{T}_{min})/\mathcal{T}_{min}$ (right) as functions of the assumed crack tip position x and y . The optimal position is depicted by the white box.

More importantly, the same analysis also provides a quantitative estimate of the stress intensity factors for both modes I and II. The singular field, which is directly measured through the amplitudes of \mathbf{v}_5 and \mathbf{v}_6 , yields the SIF when the elastic constants are known (in present case, $E = 29.2$ GPa and $\nu = 0.2$). One obtains $K_I = 0.22 \text{ MPa}\sqrt{\text{m}}$, and $K_{II} = 0.00 \text{ MPa}\sqrt{\text{m}}$. Note that the quite low value obtained for K_I is in accordance with experimental result $K_I = 0.235 \text{ MPa}\sqrt{\text{m}}$ obtained by (Abell and Lange 1998) for cement paste, with an elastic modulus of 32.4 GPa.

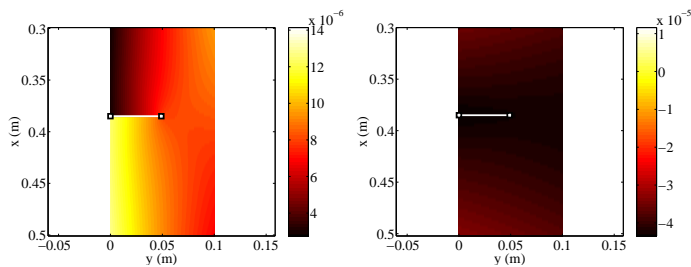


Figure 8. Identified horizontal (left) and vertical (right) components of the displacement field expressed in meters as projected onto the basis of suited functions. The crack is depicted by a white line.

5 CONCLUSIONS

During the past years, digital image correlation techniques have become a powerful tool to analyze experimental results. Measured displacement fields enriched by classical mechanical fields allow several quantities to be computed with high resolution. Following this approach, and by noting that the outputs of discrete models are similar to those obtained by experimental analyses, we propose to use DIC algorithms to post-process discrete modelings. Applications on strain field computations are shown, and a

REFERENCES

- Abell, A. and D. Lange (1998). Fracture mechanics modeling using images of fractures surfaces. *Int. J. Solids Structures* 35, 4025–4033.
- Allais, A., T. Bornert, T. Bretheau, and D. Caldemaison (1994). Experimental characterization of the local strain field in a heterogeneous elastoplastic material. *Acta Metall. Mater.* 42, 3865–3880.
- D’Adetta, G., E. Ramm, S. Diebels, and W. Ehlers (2004). A particle center based homogenization strategy for particle assemblies. *Engng. Comp.* 21, 360–383.
- Delaplace, A. and C. Rey (2005). Numerical strategies for describing material failure with discrete element model. In *ESAFORM2005*, pp. 101–104. Editor D. Banabic, the Publishing House of the Romanian Academy.
- Destuynder, P. and M. Djaoua (1981). Sur une interprétation mathématique de l’intégrale de rice en théorie de la rupture fragile. *Math. Meth. Appl. Sci.* 3, 70–87.
- Geers, M., R. de Borst, and W. Brekelmans (1996). Computing strain fields from discrete displacement fields in 2d-solids. *Int. J. Solids Structures* 33, 4293–4307.
- Hellen, T. (1975). On the method of virtual crack extensions. *Int. J. Num. Meth. Eng.* 9, 187–207.
- Kruyt, N. and L. Rothenburg (1996). Micromechanical definition of the strain tensor for granular materials. *Journal of Applied Mechanics (Transactions of the ASME)* 63, 706–711.
- Réthoré, J., A. Gravouil, F. Morestin, and A. Combescure (2005). Estimation of mixed-mode stress intensity factors using digital image correlation and an interaction integral. *Int. J. Fract.* 132, 65–79.
- Roux, S. and F. Hild (2006). Stress intensity factor measurements from digital image correlation: post-processing and integrated approaches. *Int. J. Fract.* 140, 141–157.
- Schlangen, E. and E. J. Garboczi (1997). Fracture simulations of concrete using lattice models: Computational aspects. *Eng. Fracture Mech.* 57(2/3), 319–332.
- Sutton, M., S. McNeill, J. Helm, and Y. Chao (2000). Advances in two-dimensional and three-dimensional computer vision. *Photomechanics, Springer*, 323–372.
- Tillemans, H. and H. Herrmann (1995). Simulating deformations of granular solids under shear. *Physica A* 21, 261–288.
- Van Mier, J. G. M., M. R. A. Van Vliet, and T. K. Wang (2002). Fracture mechanisms in particle composites: statistical aspects in lattice type analysis. *Mech. Mater* 34, 705–724.
- Woestyn, S., A. Delaplace, and P. Koechlin (2006). Analyse de la rupture dynamique du béton par un modèle discret. *Revue Européenne de génie civil* 10, 1281–1308.